GÉORISQUES IV GEOHAZARDS

CHARACTERIZATION AND MONITORING OF THE ÅKNES ROCKSLIDE USING TERRESTRIAL LASER SCANNING

Thierry Oppikofer
Institute of Geomatics and Risk Analysis (IGAR), University of Lausanne, Switzerland, thierry.oppikofer@unil.ch
Michel Jaboyedoff
Institute of Geomatics and Analysis of Risk (IGAR), University of Lausanne, Switzerland
Lars Harald Blikra
Åknes/Tafjord-project, Stranda, Norway
Marc-Henri Derron
Geological Survey of Norway (NGU), Trondheim, Norway

RÉSUMÉ
Le scanner laser terrestre (SLT) de longue portée est un outil puissant pour la surveillance de mouvements de versant, puisqu'il fournit une image 3D de haute résolution de la topographie. Cet article décrit de possibles analyses d'images SLT de pentes rocheuses instables. Les images SLT sont utilisées pour l'analyse structurale de l'escarpement principal vertical et inaccessible du glissement rocheux d'Åknes en Norvège, incluant la détermination des jeux de discontinuités et des axes de plis. Des déplacements déterminés à l'aide de séries temporelles de données SLT contiennent non seulement des informations sur la vitesse et la direction de déplacement (6-7 cm/an vers 185° avec un plongement de 55°), mais aussi sur des composants rotationnels, tels que le basculement (vers 327° par 0.03°). Un possible modèle de l'instabilité explique les déplacements transrationnels et rotationnels mesurés par une combinaison de glissement plan, tassement et basculement.

ABSTRACT
Long-range terrestrial laser scanning (TLS) is a powerful tool to monitor slope movements, since it provides a high-resolution 3D image of the topography. This article presents a review of the possible analyses of TLS images of instable rock slopes. The TLS images are used for the structural analysis of the steep, inaccessible main scar of the Åknes rockslide in Norway, including assessment of the discontinuity sets and fold axes. Displacements determined by a time-series analysis of TLS data provide information on movement velocities and directions (6-7 cm/year towards 185° with a plunge of 55°), as well as rotational components, like toppling (towards 327° by 0.03°). A possible instability model explains the measured translational and rotational displacements by a combination of planar sliding, sackung and toppling towards the opened graben structure.

1. INTRODUCTION

Landslides are a major natural hazard threatening the inhabitants of many mountainous regions. Population increase and extension of inhabited areas into potentially hazardous locations leads to an important increase of potential losses in the case of a disaster. The Norwegian fjords have frequently been affected by large rockslides causing catastrophic tsunamis in the narrow fjords. In the Storfjord in Norway, several historical reports and deposits in the fjord testify to this high activity with approximately one catastrophic rockslide event every 100 years (Blikra *et al.*, 2005; Blikra *et al.*, 2006c). The last major event was the 1934 Tafjord rockslide that led to a more than 60 m high tsunami wave killing 40 people (Bugge, 1937; Kaldhol and Kolderup, 1937; Braathen *et al.*, 2004).

The Åknes rockslide is situated on the western flank of Sunnylvsfjord, a branch of the Storfjord (Figure 1). Its volume was first estimated to 5 to 6 million m^3 (NGI, 1992; NGI, 1996; Braathen *et al.*, 2004). New estimations reveal a volume of more than 35 million m^3 (Blikra *et al.*, 2006b) for the whole landslide body and its failure might cause a catastrophic tsunami in the fjord (Blikra *et al.*, 2005; Harbitz and Eidsvig, 2005; Blikra *et al.*, 2006c).

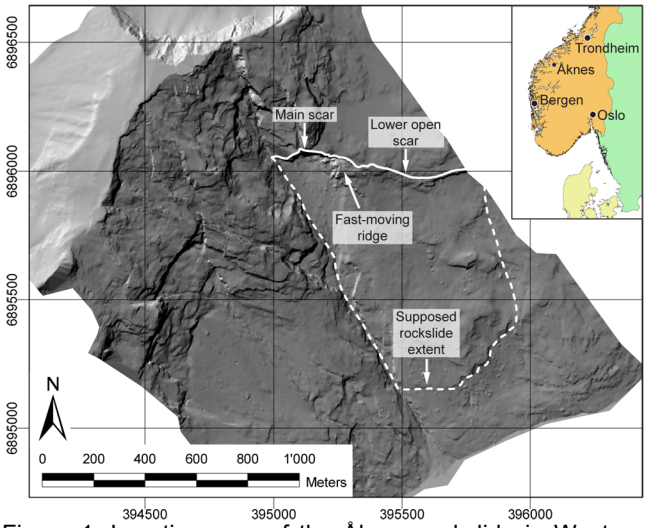

Figure 1. Location map of the Åknes rockslide in Western Norway (Shaded aerial DEM in UTM 32N coordinates from Blom Geomatics AS, © Åknes/Tafjord Project, 2005). The main features of the rockslide are outlined.

In : J. Locat, D. Perret, D. Turmel, D. Demers et S. Leroueil, (2008).
Comptes rendus de la 4e Conférence canadienne sur les géorisques: des causes à la gestion.
Proceedings of the 4th Canadian Conference on Geohazards : From Causes to Management. Presse de l'Université Laval, Québec, 594 p.

The measured slope movements reach about 4 cm/year (Braathen *et al.*, 2004; Derron *et al.*, 2005), but higher annual displacements are recorded in the most unstable parts (7-20 cm/year) (Blikra *et al.*, 2006b). Since 2005, the Åknes rockslide has been investigated and monitored as part of the Åknes/Tafjord Project (www.aknes-tafjord.no). Besides geological, structural, geophysical and borehole investigations, the monitoring focuses on the measurement of slope movements using different techniques. Some of them are point based (GPS, extensometers, total station, and laser distance meters), while others are area based (photogrammetry, radar interferometry, and aerial or terrestrial laser scanning). Point based measurements are generally more accurate than area based techniques, but provide only information on few selected monitoring points and not the whole area of a landslide (Bitelli *et al.*, 2004).

Terrestrial laser scanning is widely used nowadays for rockfall and landslide detection and monitoring (Slob and Hack, 2004; Bauer *et al.*, 2005; Biasion *et al.*, 2005; Jaboyedoff *et al.*, submitted) through the quantification of rockfall in cliff erosion (Rosser *et al.*, 2005), the back-analysis of a rockfall (Abellán *et al.*, 2006), and structural analyses or the measurement of displacements (Oppikofer *et al.*, in review). The knowledge of the displacement rates is essential for the hazard assessment (Crosta and Agliardi, 2003), especially for the evaluation of volumes, the failure prediction, and the assessment of the tsunami hazard.

Therefore a detailed investigation of the Åknes landslide was undertaken in 2006 and 2007 by terrestrial laser scanning (TLS). The primary goal of this survey was the detection of movements in the uppermost part of the landslide by comparison of time-series of TLS images. These TLS data also enabled the completion of the existing aerial Lidar data set (acquired by Blom Geomatics AS for the Åknes/Tafjord Project in 2005) with high resolution 3D images of the steep cliffs in the Åknes area, as well as the structural analysis of the scar area.

2. METHODOLOGY

2.1 Lidar technology

The terrestrial laser scanning (TLS) technology is based on time-of-flight distance measurement using an infrared laser (Slob and Hack, 2004). The Optech ILRIS-3D used for this study has a wavelength of 1500 nm. The monochromatic and nearly parallel laser beam is sent out in a precisely known direction. The pulse gets back-scattered by various objects like vegetation, houses and the terrain. The scanner then records the back-scattered pulse. The flight time of the signal is then converted into the distance between the scanner and the object.

Mirrors inside the scanner allow for scanning of a 40° wide and 40° high field of view in a single acquisition with about 2500 points per second. The 3D coordinates of each point relative to the scanner are defined by its distance and direction. At a distance of 100 m, the instrument accuracy equals approximately 7 mm for the distance and 8 mm for the position. The range depends on the target reflectivity. Objects at a distance of about 600 to 800 meters can usually be scanned. Higher distances can be reached for very good reflectors. The resolution depends on the distance of the object and the chosen angular spacing between two spots.

2.2 Data acquisition and analysis

In order to obtain a complete 3D model of an object, TLS data from different viewpoints are acquired. These raw scans need to be treated and cleaned to remove any unwanted objects, like the vegetation. The individual scans are then combined using first a manual alignment and second an automated iterative procedure in order to minimize the alignment error between two scans. Finally, the 3D image is georeferenced using an aerial laser digital elevation model (Laser-DEM) or GPS points.

Combined with aerial Lidar data, this terrestrial Lidar image completes the Laser-DEM that is generally only poorly defined in steep cliffs. The high-resolution 3D images enable structural analyses of the rock walls, like the determination of the orientation of discontinuity sets or fold axes by fitting simple geometric forms (planes, cylinders, cones) through selected points.

Time-series of TLS images allow for the detection of slope movements, like landslides or rockfalls (Bauer *et al.*, 2005; Rosser *et al.*, 2005; Abellán *et al.*, 2006; Oppikofer *et al.*, in review). Slides generally lead to an advance of the terrain relative to the initial state (positive differences), whereas rockfalls, sackung or erosion processes lead to negative differences. So, it becomes possible to identify and distinguish the moving zones.

2.3 Displacement characterization and quantification

The displacement of a block can be described by a translation, a rotation or a combination of both. An easy way to determine the movement of an object is to select corresponding points on both images. Ideal point pairs are summits of blocks or small spurs, intersections or end points of discontinuity traces etc. The vector between a point pair provides the movement direction and velocity of the point. These displacement vectors provide essential information for the modelling of landslides and the prediction of rockfall events (Oppikofer *et al.*, in review), but errors are too high for the assessment of small, centimetric displacements. This is due to the spacing between two adjacent points (generally a few cm), the measurement error of a single point, the impossibility to pick exactly the same point and neglecting the rotation in the movement analysis.

In order to assess small displacements, a roto-translation matrix technique, based on Montserrat *et al.* (2007), has been developed for this study. It takes into account not only the translation but also the rotation of individual blocks or landslide parts, and not only point pairs but all of the data points. Each individual block from the initial state scan(s) is aligned on the final state scan(s) by a semi-automatic iterative procedure. This affine transformation can be expressed by a 4x4 matrix (Eq. 1) with 3x3 terms for the rotation (r_{11} to

r_{33}), 3 terms for the translation (t_{14} to t_{34}) and a fourth line being generally {0,0,0,1} (Stephens, 2000).

$$M_{tot} = \begin{pmatrix} r_{11} & r_{12} & r_{13} & t_{14} \\ r_{21} & r_{22} & r_{23} & t_{24} \\ r_{31} & r_{32} & r_{33} & t_{34} \\ 0 & 0 & 0 & 1 \end{pmatrix} \quad [1]$$

Frequently rotations are expressed by rotation angles around the X-, Y- and Z-axis (Euler angles) (Monserrat *et al.*, 2007). To facilitate the interpretation of the rotational component for this study, the 4x4 matrix is transformed into a toppling angle and toppling direction of the block, as well as the rotation (tilt) of the block around the toppled axis (Figure 2).

The real translation, $\vec{t}$, is expressed as a vector between the block's centre point in the initial and the final state, which is obtained by multiplication of the centre point by the roto-translation matrix (Eq. 2).

$$\vec{t} = \begin{pmatrix} \Delta X \\ \Delta Y \\ \Delta Z \\ 0 \end{pmatrix} = M_{tot} \cdot \begin{pmatrix} X \\ Y \\ Z \\ 1 \end{pmatrix} - \begin{pmatrix} X \\ Y \\ Z \\ 1 \end{pmatrix} \quad [2]$$

The total transformation equals to the translation of the centre point to its final state, $\vec{t}$, followed by the rotation, M_{rot}, of the block around its centre point. The rotation component of M_{rot} is equal to the one of the 4x4 roto-translation matrix M_{tot}, while the translation components are equal to 0 (Eq. 3).

$$M_{tot} = \begin{pmatrix} r_{11} & r_{12} & r_{13} & 0 \\ r_{21} & r_{22} & r_{23} & 0 \\ r_{31} & r_{32} & r_{33} & 0 \\ 0 & 0 & 0 & 1 \end{pmatrix} \quad [3]$$

Toppling direction and rotation angle is obtained by applying this rotation to a vertical vector (Eq. 4).

$$\vec{v}_{topple} = \begin{pmatrix} x_t \\ y_t \\ z_t \\ 0 \end{pmatrix} = M_{rot} \cdot \begin{pmatrix} 0 \\ 0 \\ 1 \\ 0 \end{pmatrix} \quad [4]$$

The azimuth φ of the rotated vector gives the toppling direction, while the angle between the vector and the vertical stands for the toppling angle ϕ (Figure 2).

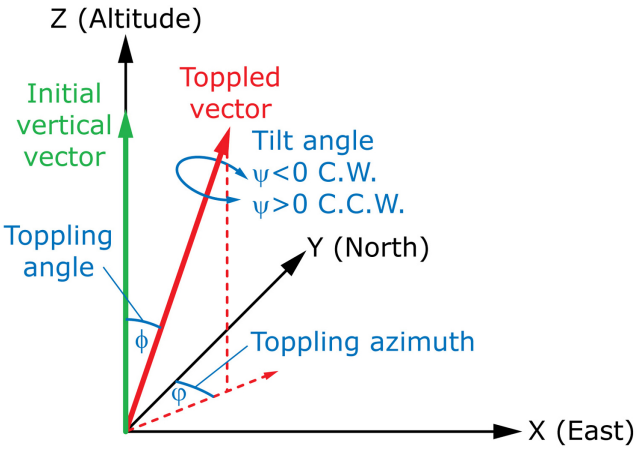

Figure 2. Scheme of the rotation components in the 3D displacement of a block. The rotation is described by the toppling azimuth and angle of an initially vertical vector and the tilt rotation around the toppled vector. Note: due to the application of the right-hand-rule, negative and positive tilt angles stand for clockwise (C.W.) and counter-clockwise (C.C.W.) rotations, respectively.

The matrix associated to this toppling M_{topple} can be calculated using the rotation by angles α and β around the x- and y-axes, respectively (Eq. 5).

$$M_{topple} = \begin{pmatrix} \cos\beta & 0 & -\sin\beta & 0 \\ 0 & 1 & 0 & 0 \\ \sin\beta & 0 & \cos\beta & 0 \\ 0 & 0 & 0 & 1 \end{pmatrix} \cdot \begin{pmatrix} 1 & 0 & 0 & 0 \\ 0 & \cos\alpha & \sin\alpha & 0 \\ 0 & -\sin\alpha & \cos\alpha & 0 \\ 0 & 0 & 0 & 1 \end{pmatrix}$$

$$M_{topple} = \begin{pmatrix} \cos\beta & -\sin\alpha \times \sin\beta & -\cos\alpha \times \sin\beta & 0 \\ 0 & \cos\alpha & \sin\alpha & 0 \\ \sin\beta & -\sin\alpha \times \cos\beta & \cos\alpha \times \cos\beta & 0 \\ 0 & 0 & 0 & 1 \end{pmatrix}$$

$$\text{with : } \alpha = -\arcsin\left(\frac{y_t}{\sqrt{y_t^2 + z_t^2}}\right) \text{ and } \beta = \arcsin\left(\frac{x_t}{\sqrt{x_t^2 + z_t^2}}\right) \quad [5]$$

Finally, the tilt angle ψ around this toppled vector is calculated by an iterative procedure recreating the tilt matrix M_{tilt} (Baker, 2002), which is obtained from the total rotation matrix M_{rot} and the toppling matrix M_{topple} (Eq. 6).

$$M_{rot} = M_{topple} \cdot M_{tilt} \quad \rightarrow \quad M_{tilt} = M_{topple}^{-1} \cdot M_{rot} \quad [6]$$

The error on the calculated movement is estimated by repeated alignment (20 times) of a block from the initial to the final state. The repeatability (1σ) for the translation magnitude and direction is better than 1 mm and 0.7°.These values are much better than values generally obtained using the point pair method described above (±5° to ±10° on the azimuth and ±7 to ±10 cm on the magnitude). For the toppling the repeatability is ~1° for the toppling direction φ

and 0.002° for the toppling angle ϕ. Repetitive calculations of the tilt angle ψ provided a mean error of 0.005°.

3. DATA SETS

On August 3 and 4, 2006 a complete 3D image of the upper main scar and the fast-moving ridge, shown in Figure 1, was obtained by TLS from the SW and NE rim of the Åknes landslide area. The lower part of the main scar was scanned from two viewpoints on the landslide body. The main scar and the ridge were again scanned on September 10, 2006. During the 2007 field campaign the main scar and the ridge were scanned on August 2, 2007 from the NE rim and on August 7, 2007 from the SW rim. The lower back crack was also scanned again on August 7, 2007.

The mean resolution on the rock face ranges between 2.5 and 12.2 centimetres. The alignment of the individual scans was performed by an iterative procedure in a specialized point cloud treatment software leading to a mean alignment error of less than 1.0 mm with a mean standard deviation of 19.7 mm. The georeferencing of the point clouds was achieved by an alignment onto the aerial Lidar point cloud acquired by Blom Geomatics AS for the Åknes/Tafjord Project in September 2005, leading to an absolute positioning error of 14 cm (1σ), whereas the relative precision of the XYZ points is about 1 cm.

4. STRUCTURAL ANALYSIS

The main scar of the Åknes landslide is approximately 200 m high and 300 m large. Difficult access and rockfall activity impede structural measurements at the bottom of the scar. Terrestrial laser scans of the scar are therefore used for the analysis of the main structural features.

4.1 Fold axis

Several folds are visible on the main scar. Assuming the folds are cylindrical, allows modelling by fitting cylinders through the TLS points of the folds (Figure 3a). The fold axes have a mean orientation of 123°/18° (trend/plunge) with only small variability (1σ = 5.7°). This fold axis orientation is in agreement with the "*gently ESE-plunging axis*" reported by Braathen *et al.* (2004).

4.2 Discontinuity sets

At different parts of the Åknes main scar and its surroundings, orientations of planar surfaces were determined. More than 100 discontinuities were measured and attributed to one of six discontinuity sets (Figure 3b).

The discontinuity set D1 has a very constant orientation (mean dip direction/dip angle: 008°/87°; 1σ = 8.5°) and no significant differences between the upper and the lower part of the main scar. The second set (249°/82°) shows slightly different fracture orientations (14°) between the upper part and the lower and right part. The distinction of these planes into two sets (D2 and D2' with mean orientations of 252°/80° and 239°/86°, respectively) leads to smaller orientation variability (9.8° and 9.3°, respectively). The discontinuity sets D3 (060°/26°) and D4 (167°/40°) show quite large distributions (1σ variability of 10.2° and 11.2°, respectively), but no significant differences are observable between the different regions of the main scar. The discontinuity set D4 stands probably for the foliation planes. The discontinuity sets D5 (292°/87°) and D6 (312°/89°) can be separated into two sets since they occur next to each other with a neat intersection line. They have both very homogenous orientations (1σ variability of 8.0° and 7.6°, respectively).

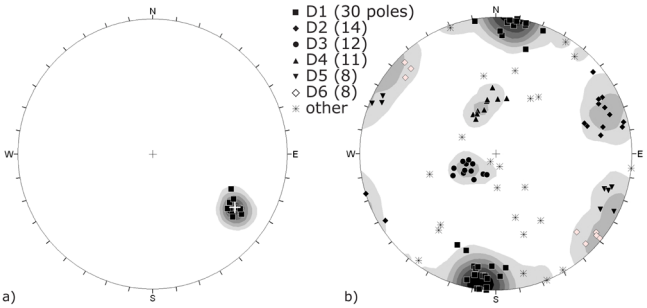

Figure 3. Lower hemisphere density stereonet of a) the fold axis orientations (squares) and the average fold axis orientation (cross); b) 106 poles of discontinuities attributed to one of the six discontinuity sets (D1 to D6).

5. MOVEMENT ANALYSIS

5.1 Comparison August 3, 2006 to September 10, 2006

For the fast-moving ridge at the Åknes landslide, the comparison of the scans taken in the beginning of August and the middle of September 2006 reveals small displacements (approximately 1 to 2 cm) towards the SE on the fast-moving ridge structure. The displacement of the ridge between August 3 and September 10, 2006 was analysed using the roto-translation matrix technique which was applied to the entire ridge area. This analysis reveals a global displacement of 13 mm towards 112°/18° (trend/plunge). The toppling component is very small (0.007° towards 023°), while the tilt angle (–0.001°) can be neglected. A more detailed analysis of the slope movement is not suitable because of the small displacements, which might lead to errors and misinterpretations.

5.2 Comparison August 3, 2006 to August 7, 2007

The scans from August 3, 2006 and August 7, 2007 were compared in order to obtain the annual displacements for the upper scar with the fast-moving ridge and for the lower scar of the Åknes landslide (see Figure 1 for localization).

5.2.1 Fast-moving ridge

For the upper part with the graben and ridge structure, this comparison reveals a movement of the ridge towards the South. The amplitude reaches 6 to 8 cm horizontally (green to yellow colours on the south-facing cliffs of the ridge) and the downward component equals 4 to 6 cm (light blue colours on the top of the ridge) (Figure 4). The comparison

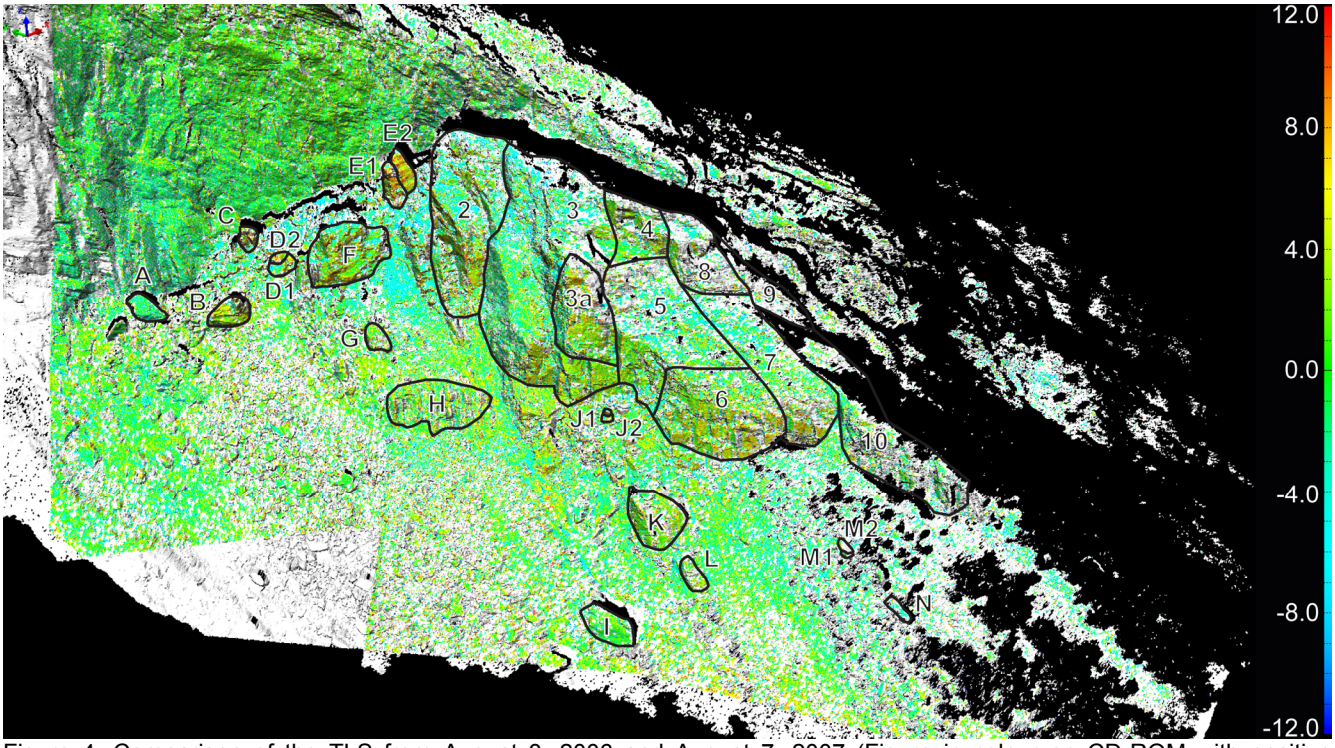

Figure 4. Comparison of the TLS from August 3, 2006 and August 7, 2007 (Figure in colour on CD-ROM with positive differences up to 12 cm shown in yellow to red, and negative differences up to 12 cm in light to dark blue). The 10 regions on the fast-moving ridge (Ridge 1 is hidden by region Ridge 2) and 13 visible blocks are outlined (Blocks O, P1 and P2 are outside the image).

image reveals also some faster movements for blocks in the graben area, like the blocks E1 and E2 (~12 cm) (Figure 4). The slight displacements apparent in the main scar are probably due to interpolation artefacts or small atmospheric influences, which cannot be avoided nor corrected. Nonetheless, since these errors are much smaller than the detected movements, they can be neglected.

For the detailed analysis of the displacements, the fast-moving ridge was divided into 11 uniformly moving regions on the basis of the TLS comparison (Figure 4). 16 blocks lying at the foot of the main scar or of the ridge were also analyzed. For each region or block a mesh of the 2006 TLS scans was created and aligned onto the 2007 scans. Using the roto-translation matrix technique, the complete 3D movement of each individual region or block is calculated.

The translation vector of the centre points of the different parts of the ridge varies significantly in length and direction (Figure 5a). Ridge 1 must not be taken into account in the global movement of the ridge, since it seems to be a detached block that is toppling (toppling angle of 0.3°) towards the graben structure in the North. The yearly displacements of the other parts of the ridge vary between 49 and 89 mm, but no clearly faster moving part is detectable.

The azimuth (trend) of the translation vectors ranges from 159° (SSE) to 217° (SSW), which correspond to the mean aspect of the slope (178°). The plunge of the vector is also quite variable with values between 38° and 61°, which are all steeper than the mean slope angle in that area (37°). Similar to the amplitude of the displacement vector, the differences in its orientation are not coherent over the different parts of the ridge. Thus, the best description of the ridge's movement can be given by the average of the displacement vectors without the Ridge 1 block (185°/55°, L = 67 mm) or the mean value weighted by the number of points contained in each part of the ridge (186°/55°, L = 61 mm). These calculated displacements are slightly lower than the differences visible in the comparison image (Figure 4).

Except for blocks Ridge 3a and Ridge 10 that are toppling towards the South, the blocks topple towards the North (between 333° and 43°) (Figure 5b). Besides the block Ridge 1, toppling angles are very low (< 0.1°) with a mean angle of 0.03°. Nonetheless, a toppling by 0.03° of a 25 m high block, as found on the ridge in Åknes landslide, leads to a displacement of 13 mm for the top of the block. Therefore, even the small toppling angles can explain the higher displacements detected in the comparison image (Figure 4). The tilt angles, i.e. the rotation of the block around the toppled normal axis, are insignificantly low (generally <0.02°).

The individual blocks in the surroundings of the ridge (Block A to Block P2) show a quite heterogeneous displacement pattern. The total amount of translational displacement

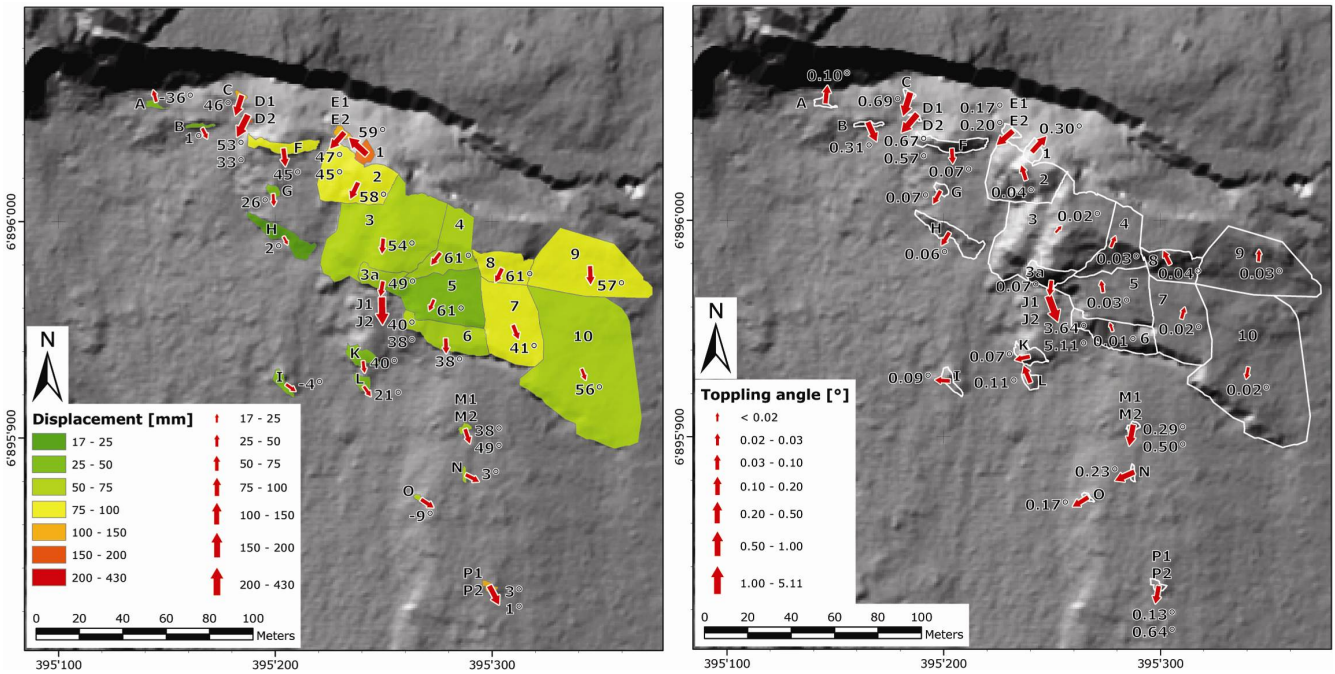

Figure 5. Map of the 11 regions on the ridge (numbers) and the 16 blocks (capital letters): a) the arrows indicate the direction and amplitude of the displacement vector for each part. The numbers next to the arrows stand for the plunge of the vector; b) shows the toppling direction (indicated by the direction of the arrow) and the toppling angle (indicated by the length of the arrow and the number). Note that a non-linear scale is used for the arrows.

ranges between 17 mm (Block H) and 430 mm (Block J2) in 1 year (Figure 5a). The movement direction is generally SE to South (between 117° and 213°), except Block A that is moving towards 343°, which is probably erroneous. The blocks mainly slide along the mean slope direction of the topography.

Several blocks have very low or negative plunge angles for the translation vectors. A negative plunge angle signifies an upward movement of the block that is hardly possible in a landslide context. They are perhaps related to alignment errors between the two TLS images, which were aligned on the points of main scar and other stable parts. Slight alignment errors become amplified with increasing distance from the main scar, like for blocks I, N, O, P1 and P2. The low plunge angles of blocks A, B and H, as well as the erroneous trend of the translation vector for Block A are probably due to the small amount of displacement of 42, 47 and 17 mm, respectively. The plunge angles of the other blocks range between 21° (Block L) and 61° (Block F) and are coherent with the plunge angles of the ridge.

Toppling angles of the blocks are usually higher than on the ridge (between 0.05° and 5.1°) probably due to the rolling of the blocks on the scree slope. The toppling direction is quite variable, but generally orientated downslope. The tilt angles are also higher than for the ridge (up to 3.5° for Block J2), but their signification in terms of sliding, toppling or rotation remains difficult to interpret.

For the ridge in the uppermost part of the Åknes landslide, Braathen *et al.* (2004) stated that "*transport is parallel to the surface, which dips 30-40° to the south*". The displacement

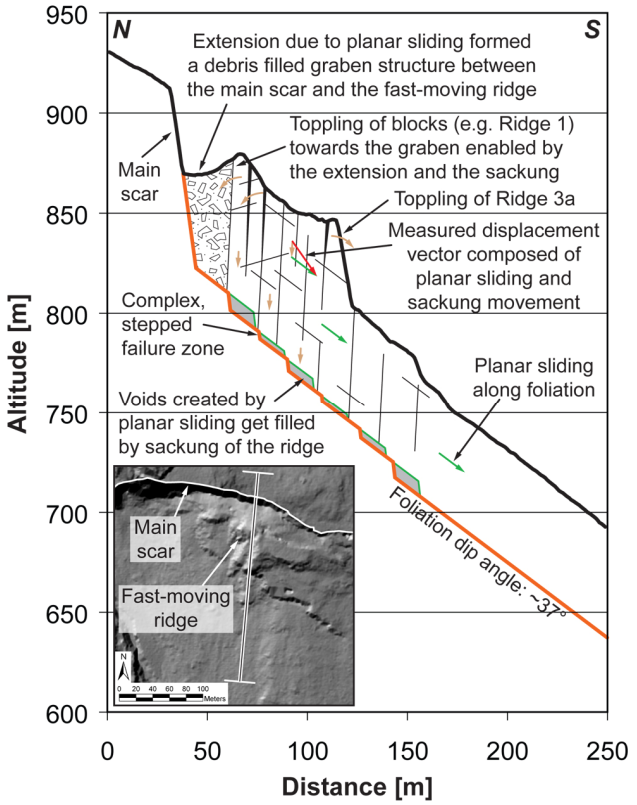

Figure 6. Schematic profile across the upper part the Åknes rockslide (based on aerial Lidar DEM (© Åknes/Tafjord Project) explaining the measured displacement vectors and the toppling at the front of the ridge and towards the graben.

direction is confirmed by these TLS measurements, but the obtained plunge of the translation vector is significantly higher. This more important downward movement is probably caused by the sackung of the uppermost part of the Åknes rockslide filling the voids opened in a complex, stepped failure zone by the planar sliding along the foliation (Figure 6). The evoked stepped failure zone is mainly due to the preferential rupture along the hinges of the isoclinal folds, as observed in the main scar of the Åknes rockslide, and along the foliation, which is subvertical in the main scar area, but becomes more moderately dipping in the middle and lower part of the landslide (Blikra *et al.*, 2006a).

The planar sliding parallel to the foliation plane induced the creation of a graben structure between the main scar and the fast-moving ridge. This graben is partially filled with debris, but allows blocks that are delimited by discontinuity sets D1 (rear), D3 (basal), and D5 (lateral) to topple towards the graben. This toppling in addition to the sackung explains the measured rotational movements of the ridge towards the North. The part Ridge 3a is delimited by discontinuity sets D1 (rear), D4 (basal), and D5 (lateral) and is able to topple-slide towards the South, which is supported by the TLS data. Finally, it is the planar sliding mechanism that leads to the apparent rotational movements of the uppermost part.

5.2.2 Lower scar

The rock mass below the lower scar (NE of the lateral transfer fault) shows approximately 1 cm horizontal and 1 cm vertical displacement (Figure 7). On the other hand the area SW of the transfer fault reveals an advance of the rock mass by about 3 cm in one year, which is slightly lower but comparable to the displacement of the ridge. The part above the lower scar, that is supposed to be stable in this comparison, shows no significant displacements (apparent displacements varying between –1 and +1 cm).

The matrix alignment technique is also used for the area below the lower scar, as well as the area SE of the lateral transfer fault. The first one reveals a translational displacement of 9 mm toward 244°/42° accompanied by a toppling of 0.01° towards 352°, while the second region provides an overall translation of 21 mm toward 163°/23° and a toppling direction towards 023° by 0.01°.

These movements are consistent with the extension of the lower scar parallel to the main sliding direction given by the mean translation of the ridge. The slope movements of the region in the SW of the transfer fault are also coherent with the ridge displacement. The decrease in toppling indicates that sackung and toppling are quite important mechanisms in the uppermost part of the landslide (fast-moving ridge), but play only a minor role in the middle part of the Åknes landslide.

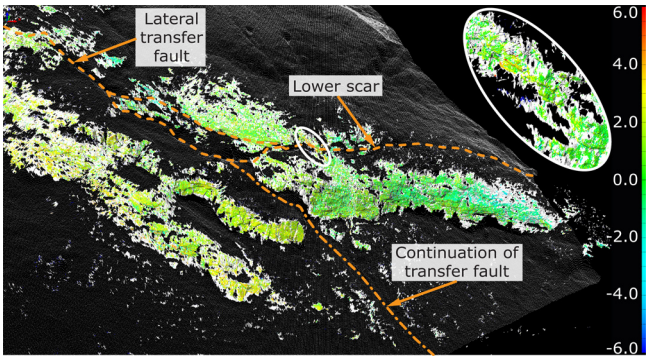

Figure 7. View towards the North of the lower scar area showing the comparison image of the 2006 and 2007 TLS data (colour figure on CD-ROM shows positive differences (up to 6 cm) with yellow to red colours, and negative differences (up to –6 cm) in blue tones). The extension fracture at the lower scar and the lateral transfer faults are shown as a stippled line, while its continuation is represented as a dash-dotted line. The enlargement shows a zone next to the lower scar that displays higher deformation (colour scheme shows differences between –20 and +20 cm).

6. CONCLUSIONS & PERSPECTIVES

The terrestrial laser scanner survey of the upper part of the Åknes landslides shows the huge potential of this new method. TLS provides high resolution 3D images of the topography which complement the DEM generated from aerial laser scanning, that often lack precise information in the steep cliffs. The TLS data of inaccessible cliffs, like the main scar of the Åknes landslide, enable a detailed analysis of the main structural features of a cliff, like major discontinuity sets and fold axes.

More important for landslide hazard assessment and landslide monitoring is the potential of TLS to detect slope movements over a whole landslide area and not only on single monitoring points. In contrast to many other monitoring techniques, TLS provides information not only on the total amount of displacement, but also on the type of movement, i.e. translation and/or rotation.

The improved roto-translation technique is very useful for the displacement measurement and the interpretation of the movement in terms of landslide mechanism. The measured displacements are consistent with the overall movement of the landslide. A possible rockslide mechanism model, including planar sliding, as well as toppling and sackung components for the uppermost part of the Åknes rockslide, was established on the basis of the TLS data. This model still needs to be tested and confronted to other models based on structural and geomorphologic observations, as well as on geophysical investigations.

The comparison of TLS images of the upper part of the Åknes landslide reveals displacements as low as 1 cm and up to several decimetres. In contrast to other area-based monitoring techniques, the range of measurable displacements by TLS is very large which opens a wide range of

landslide monitoring applications. TLS also provides rapidly precise 3D topography information for quick hazard assessment in emergency situations.

7. ACKNOWLEDGMENTS

The authors wish to thank Magali Frayssines, Mathias Dessimoz and Andrea Pedrazzini for aid during fieldwork, as well as Jean Hutchinson (Queen's University, Kingston, Canada) and Réjean Couture (Geological Survey of Canada) for their evaluation of this manuscript and their valuable comments.

8. REFERENCES

Abellán, A., Vilaplana, J.M. and Martínez, J. 2006. Application of a long-range Terrestrial Laser Scanner to a detailed rockfall study at Vall de Núria (Eastern Pyrenees, Spain). Engineering geology, Vol. 88(3-4), pp. 136-148.

Baker, M. 2002. 3D World Simulation - Maths - Axis Angle to Matrix. http://www.euclideanspace.com/maths/geometry/rotations/conversions/angleToMatrix/index.htm.

Bauer, A., Paar, G. and Kaltenböck, A. 2005. Mass Movement Monitoring Using Terrestrial Laser Scanner for Rock Fall Management. In: van Oosterom, P., Zlatanova, S. and Fendel, E.M. (Editors), Geo-information for Disaster Management. Springer, Berlin, pp. 393-406.

Biasion, A., Bornaz, L. and Rinaudo, F. 2005. Laser Scanning Applications on Disaster Management. In: van Oosterom, P., Zlatanova, S. and Fendel, E.M. (Editors), Geo-information for Disaster Management. Springer, Berlin, pp. 19-33.

Bitelli, G., Dubbini, M. and Zanutta, A. 2004. Terrestrial Laser Scanning and Digital Photogrammetry Techniques to Monitor Landslide Bodies, Proceedings of the XXth ISPRS Congress, Istanbul, International Society for Photogrammetry and Remote Sensing, pp. 246–251.

Blikra, L.H., Anda, E., Belsby, S., Jogerud, K. and Klempe, Ø. 2006a. Åknes/Tafjord prosjektet: Statusrapport for Arbeidsgruppe 1 (Undersøking og overvaking), Åknes/Tafjord project, Stranda, Norway.

Blikra, L.H., Anda, E., Høst, J. and Longva, O. 2006b. Åknes/Tafjord-prosjektet: Sannsynlighet og risiko knyttet til fjellskred og flodbølger fra Åknes og Hegguraksla. 2006.039, Geological Survey of Norway, Trondheim.

Blikra, L.H., Longva, O., Braathen, A., Anda, E., Dehls, J.F. and Stalsberg, K. 2006c. Rock Slope Failures in Norwegian Fjord Areas: Examples, Spatial Distribution and Temporal Pattern. In: Evans, S.G., Scarascia Mugnozza, G., Strom, A. and Hermanns, R.L. (Editors), Landslides from Massive Rock Slope Failure. NATO Science Series, IV. Earth and Environmental Sciences, Vol 49. Springer, Dodrecht, Netherlands, pp. 475-496.

Blikra, L.H., Longva, O., Harbitz, C. and Løvholt, F. 2005. Quantification of rock-avalanche and tsunami hazard in Storfjorden, western Norway. In: Senneset, K., Flaate, K. and Larsen, J.O. (Editors), Landslides and Avalanches: ICFL 2005 Norway. Taylor & Francis Group, London, pp. 57-64.

Braathen, A., Blikra, L.H., Berg, S.S. and Karlsen, F. 2004. Rock-slope failure in Norway; type, geometry, deformation mechanisms and stability. Norwegian Journal of Geology, Vol. 84(1), pp. 67-88.

Bugge, A. 1937. Fjellskred fra topografisk og geologisk synspunkt. Norsk Geografisk Tidsskrift, Vol. VI, pp. 342-360.

Crosta, G.B. and Agliardi, F. 2003. Failure forecast for large rock slides by surface displacement measurements. Canadian Geotechnical Journal, Vol. 40(1), pp. 176-191.

Derron, M.H., Blikra, L.H. and Jaboyedoff, M. 2005. High resolution digital elevation model analysis for landslide hazard assessment (Åkerneset, Norway). In: Senneset, K., Flaate, K. and Larsen, J.O. (Editors), Landslides and Avalanches: ICFL 2005 Norway. Taylor & Francis Group, London, pp. 101-106.

Harbitz, C.B. and Eidsvig, U. 2005. Åknes/Tafjord-prosjektet: Innledende numeriske analyser av flodbølger som følge av mulige skred fra Åkneset, Norges Geotekniske Institutt NGI, Oslo, Norway.

Jaboyedoff, M., Oppikofer, T., Locat, A., Locat, J., Turmel, D., Robitaille, D., Demers, D. and Locat, P. submitted. Use of ground-based Lidar for the analysis of retrogressive landslides in sensitive clay and of rotational landslides in river banks. Canadian Geotechnical Journal.

Kaldhol, H. and Kolderup, N.-H. 1937. Skredet i Tafjord 7. april 1934. Bergens museums Årbok. Naturvidenskapelig rekke, Bergen, Norway, 11 pp.

Monserrat, O., Jaszczak, P. and Crosetto, M. 2007. Deformation measurement based on terrestrial laser scanner data. In: Grün, A. and Kahmen, H. (Editors), Optical 3-D Measurement Techniques VIII, Zürich, Switzerland, ETH Zürich, pp. 249-256.

NGI 1992. Skredgenererte bølger - En teoretisk gjennomgang med praktiske eksempler. 894031-1, Norwegian Geotechnical Institute, Oslo.

NGI 1996. Åkernes Landslide - General Description of the Åkernes Slide Area and Control Measures. 585910-9, Norwegian Geotechnical Institute, Oslo.

Oppikofer, T., Jaboyedoff, M. and Keusen, H.-R. in review. The Eiger collapse–an example of how climate change impacts relief. Nature Geosciences.

Rosser, N.J., Petley, D.N., Lim, M., Dunning, S.A. and Allison, R.J. 2005. Terrestrial laser scanning for monitoring the process of hard rock coastal cliff erosion. Quarterly Journal of Engineering Geology and Hydrogeology, Vol. 38(4), pp. 363-375.

Slob, S. and Hack, R. 2004. 3D Terrestrial Laser Scanning as a New Field Measurement and Monitoring Technique. In: Hack, R., Azzam, R. and Charlier, R. (Editors), Engineering Geology for Infrastructure Planning in Europe. A European Perspective. Lecture Notes in Earth Sciences. Springer, Berlin / Heidelberg, pp. 179-190.

Stephens, R. 2000. Three-Dimensional Transformations, Visual Basic Graphics Programming. John Wiley & Sons, New York, pp. 419-464.